J Neuropathol Exp Neurol
Vol. 78, No. 5, May 2019, pp. 389–397
doi: 10.1093/jnen/nly124

ORIGINAL ARTICLE

Expression of GLUT1 in Pseudopalisaded and Perivascular Tumor Cells Is an Independent Prognostic Factor for Patients With Glioblastomas

Satoru Komaki, MD, Yasuo Sugita, MD, Takuya Furuta, MD, Kyohei Yamada, MD, Mayuko Moritsubo, MD, Hideyuki Abe, PhD, Jun Akiba, MD, Naohisa Miyagi, MD, Hideo Nakamura, MD, Hiroaki Miyoshi, MD, Koichi Ohshima, MD, and Motohiro Morioka, MD

Abstract

Glioblastomas are highly aggressive brain tumors with a particularly poor prognosis. Glucose transporter-1 (GLUT1/SLC2A1), a uniporter that is expressed by various carcinomas and may be involved in malignant neoplasm glycometabolism, may also be related to prognosis in glioblastomas. GLUT1 is essential to central nervous system glycometabolism. To clarify the exact role of GLUT1 in glioblastoma, we assessed the expression and localization of GLUT1 in patient samples by immunohistochemistry and in situ RNA hybridization. This revealed that GLUT1 was mainly expressed on perivascular and pseudopalisaded tumor cell membranes. All samples expressed GLUT1 to some degree, with 30.8% showing stronger staining. On the basis of these data, samples were divided into high and low expression groups, although *SLC2A1* mRNA expression was also higher in the high GLUT1 expression group. Kaplan-Meier survival curves revealed that high GLUT1 expression associated with lower overall survival (log-rank test, $p = 0.001$) and worse patient prognoses ($p = 0.001$). Finally, MIB-1 staining was stronger in high GLUT1 expression samples ($p = 0.0004$), suggesting a link with proliferation. We therefore hypothesize that GLUT1 expression in glioblastomas may enhance glycolysis, affecting patient prognosis. Examination of GLUT1 in patients with glioblastomas may provide a new prognostic tool to improve outcome.

Key Words: Angiogenesis, Glioblastomas, Glucose transporter (GLUT), Warburg effect.

INTRODUCTION

The glucose transporter (GLUT) protein family contains various important molecules that use glucose diffusion gradients (and those of other sugars) for transport across the plasma membrane. They exhibit various substrate specificities, kinetic properties, and tissue expression profiles, depending on their role (1). The GLUT protein family belongs to a larger facilitator superfamily of membrane transporters (2); 13 related members of the SLC2A (GLUT) protein family have been identified in humans (3). Structurally, these molecules are divided into 3 classes; GLUT1–4 (class 1); GLUT5, 7, 9, and 11 (class 2); and GLUT6, 8, 10, and 12 (class 3) (2). In the central nervous system, GLUT1 plays a critical role in cerebral glucose uptake and is the major GLUT isoform expressed in brain endothelial cells and brain astrocytes. It has been suggested that GLUT1 supplies glycolytically derived lactate to neurons as a major fuel source (4, 5). The protein is a 492-amino-acid uniporter that is expressed by endothelial cells of the blood-brain barrier. In humans, it is encoded by the *SLC2A1* gene (6) and the GLUT1 protein possesses 12 transmembrane segments, a single site of N-linked glycosylation, a relatively large, central cytoplasmic linker domain; it also exhibits a topology where both the N and C terminals are positioned in the cytoplasm (6). In 1996, Younes et al reported that GLUT1 expression in colorectal carcinomas associated with high incidence rates of lymph node metastasis (7). Subsequently, numerous studies have reported contradictory evidence of the relationship between GLUT1 expression and prognosis in solid human tumors (8–14). Of note is a comprehensive meta-analysis of 2948 patients across 26 different studies that indicated that GLUT1 expression was a promising biomarker for prognosis, consistently showing an association with overall survival at 3 and 5 years (15). Among the tumor types evaluated, higher expression of GLUT1 in tumor tissues was also linked to worse overall survival at 3 and 5 years in oral squamous cell carcinomas and breast cancers (15). The expression of GLUT1 in astrocytomas and glioblastomas has also been reported to correlate with hypoxia-inducible factor-1 (HIF-1) in pseudopalisades, suggesting a link to hypoxia (16–20). However, the exact role of GLUT1 in tumorigenesis remains to be elucidated in highly aggressive glioblastomas.

From the Departments of Pathology (SK, YS, TF, KY, MM, HM, OK); Neurosurgery (SK, NM, HN, MM); and Diagnostic Pathology (HA, JA), Kurume University School of Medicine, Kurume, Fukuoka, Japan.
Send correspondence to: Satoru Komaki, MD, Department of Neurosurgery, Kurume University School of Medicine, Asahimachi 67, Kurume, Fukuoka 830-0011, Japan; E-mail: komaki_satoru@med.kurume-u.ac.jp
This research did not receive any specific grant from funding agencies in the public, commercial, or not-for-profit sectors.
The authors have no duality or conflicts of interest to declare.
Supplementary Data can be found at academic.oup.com/jnen.

To address this, we analyzed the expression of GLUT1 in IDH wildtype, World Health Organization (WHO) grade IV glioblastomas and any correlation with patient prognosis.

MATERIALS AND METHODS

Patient Samples

Surgically collected tissue samples from 52 patients with glioblastomas were analyzed. All tumor specimens were retrieved from the archives of Kurume University Hospital, Kurume, Japan between 2010 and 2016. The study was performed in accordance with the principles of the Helsinki Declaration and was approved by the institutional ethics committee. All specimens were histologically diagnosed as IDH-wildtype glioblastoma using WHO criteria (21). Multivariate survival analysis was used to assess the significance of various prognostic factors, including complete resection, radiotherapy, age (>18 years), Karnofsky performance status (KPS) scores, and the expression of GLUT1.

Immunohistochemistry

Tissue samples were fixed in 10% buffered formalin, embedded in paraffin, and processed using conventional histological and immunohistochemical methods. Five-micrometer-thick sections were stained with hematoxylin and eosin for histological evaluation. The remaining unstained serial sections were used for immunohistochemistry analysis following heat-induced antigen retrieval. These were stained with the appropriate antibodies and expression was evaluated with immunoperoxidase (ChemMate ENVISION kit/HRP[DAB]; DakoCytomation, Carpinteria, CA) using a Dako Autostainer Universal Staining System (DakoCytomation). The primary antibodies used were antiGLUT1 (1:3200; Abcam, Cambridge, UK), anti-endoglin (CD105; 1:50; Novocastra, Newcastle, UK), and antiKi-67 (MIB-1; 1:100; Immunotech, Marseille, France). MIB-1 labeling indices were determined as the percentage of the nuclear area stained in areas of maximal labeling. GLUT1 expression in glioblastomas was evaluated as both staining intensity and the number of stained cells by 2 observers in independent examinations. Samples that varied significantly between the 2 observers were re-evaluated to arrive at a consensus.

Fluorescence Immunohistochemical Staining

Fluorescence double immunostaining of GLUT1 and other markers (HIF1α, CD34, and Ki67) in tumor tissues was performed. Double staining was performed in a glioblastoma sample with antiGLUT1 (1:100, Thermo Fisher, UK), antiKi67 (1:100, Dako, Glostrup, Denmark), and antiCD34 (1:100, Leica, Milton Keynes, UK) antibodies followed by addition of antirabbit IgG-Texas Red (TR; sc-2780, Santa Cruz Biotechnology, Santa Cruz, CA), and antimouse IgG-Alexa488 (Life Technologies, Carlsbad, CA). Assessment of staining colocalization was performed using the OPAL 7-color fIHC Kit (Perkin Elmer, Waltham, MA) according to the manufacturer's protocols. Fluorescence was measured using a fluorescent microscope (BX51FL, Olympus, Tokyo, Japan) and a charged-coupled device camera (DP71, Olympus).

TABLE 1. Primer Design and PCR Product

Gene	Primer Sequence	Product
IDH1	Forward: 5′-GGTTGAGGAGTTCAAGTTGAAACAAAT-3′	244 bp
	Reverse: 5′-CACATACAAGTTGGAAATTTCTGGGCC-3′	
IDH2	Forward: 4′-GGGGTTCAAATTCTGGTTGAAAGATGG	289 bp
	Reverse: 5′-TAGGCGAGGAGCTCCAGTCGGG-3′	

DNA Isolation and Mutation Analysis

The mutational statuses of *IDH1* and *IDH2* were determined by Sanger sequencing. Briefly, genomic DNA was isolated from the relevant formalin-fixed paraffin-embedded (FFPE) tissue blocks by cutting 10-μm-thick sections, followed by extraction using a QIAamp DNA Micro Kit (Qiagen, Hilden, Germany). *IDH1* exon 4 and *IDH2* exon 4 were amplified by polymerase chain reaction (PCR) with the indicated primers (Table 1). The amplifying conditions for *IDH1* and *IDH2* were both an initial denaturing step of 95°C for 10 minutes, followed by 40 cycles of denaturation at 95°C for 30 seconds, an annealing step at 60°C for 30 seconds, and then extension at 72°C for 30 seconds, with a final extension at 72°C for 10 minutes. PCR products were separated on 2% agarose gels by electrophoresis, excised and then sequenced on an ABI PRISM 310 Genetic Analyzer (Life Technologies, Gaithersburg, MD). Analyses of sequence data were performed using GENETYX software Ver. 10 (GENETYX, Tokyo, Japan) and a reference sequence complementary to each gene.

RNAscope

SLC2A1 (*GLUT1*) mRNA in situ hybridization was performed using an RNAscope 2.5 HD Assay Kit-BROWN (ACD, Newark, CA), according to the manufacturer's protocols. Tissue sections, 2.5-μm thick, were deparaffinized in xylene and dehydrated through an ethanol series. The sections were then incubated in citrate buffer (10 nmol/L, pH 6.0) and maintained at 100–103°C for 15 minutes using a hot plate. They were then rinsed in deionized water and immediately treated with 10 μg/mL protease (Sigma-Aldrich, St. Louis, MO) at 40°C for 30 minutes in a HybEZ hybridization oven (Advanced Cell Diagnostics, Hayward, CA). Hybridization with target probes, preamplifier, amplifier, label probes, and chromogenic detection were performed as previously described for cultured cells. RNAscope scores and the heterogeneity of *SLC2A1* mRNA signals were estimated using the manufacturer's recommended protocols and a semiquantitative scoring system. The staining scores were as follows: 0, no staining or <1 dot to every 10 dots; staining score 1, 1–3 dots/cell; staining score 2, 4–10 dots/cell or very few dot clusters; staining score 3, >10 dots/cell and <10% positive cells with clusters; staining score 4, >10 dots/cell and 10% positive cells with clusters. The evaluation was performed by 3 observers (S.K., Y.S., and K.Y.) across independent examinations.

Cell Culture

Human glioma cell lines T98, U87, and U251 were obtained from American Type Culture Collection in 2009. Authentication of the cell lines was unnecessary because cells were expanded by culturing them for <2 passages and stored at −80°C. Low-passage cells were used for experiments within 6 months after resuscitation. They were maintained in Dulbecco's modified Eagle medium supplemented with 10% fetal bovine serum (FBS), 100 U/mL penicillin, and 100 μg/mL streptomycin.

Cell Viability and Cell Proliferation

Cell proliferation was evaluated in triplicates by a colorimetric WST-1 assay (Roche, Mannheim, Germany) according to the manufacturer's protocol. Approximately 1000 cells of each population were seeded in 96-well plastic plates in 200 μL of culture medium supplemented with 0.1% FBS. The plates were incubated for 4 hours at 37°C. Twenty microliters of WST-1 (10% of total volume) was added to the cells, and the cells were incubated. The plate was read using DS2 (Dynex Technologies, Chantilly, VA) by measuring the absorbance of the dye at 450 nm, with 600 nm set as the reference wavelength. Averages of the absorbance values were calculated and plotted. The cells were treated with various concentrations of WZB-117 (Sigma-Aldrich, Munich, Germany), a specific GLUT-1 inhibitor.

Statistical Analysis

To reveal any correlation between the expression of GLUT1 in glioblastomas and patient prognoses, statistical analysis among the relevant groups was performed using JMP13 (SAS Institute Inc., Cary, NC). Survival rates were computed using Kaplan-Meier curves. Patients were excluded if they were lost to follow-up at the time of analysis. Cox proportional hazards regression models were used for multivariate analyses of overall survival. In addition, Kendal tau rank correlation tests were performed between GLUT1 expression, Ki-67 labeling indices, and the number of CD105 (endoglin) positive vessels in glioblastomas. Statistical significance was set at a threshold of $p < 0.05$.

Gene Expression Database

Information regarding SLC2A1 alterations and patient's survival time in glioblastomas was downloaded from the Cancer Genome Atlas (TCGA) Database, an open access database that is publicly available at http://www.cbioportal.org (22, 23). Six hundred and four glioblastoma cases (TCGA, Provisional) were selected. These cases were divided into 2 groups: SLC2A1 mRNA upregulated or not altered. Gene altered cases were defined as that expression level of SLC2A was observed greater than standard deviation from the mean. The proportion of upregulated cases was calculated and overall survival and progression-free survival were estimated by Kaplan-Meier analysis. Furthermore, co-expression genes with SLC2A1 in glioblastomas were investigated by calculating Spearman's correlation coefficients. We selected vascular endothelial growth factor (VEGF) as the neoangiogenic marker, CD44 as the mesenchymal marker, PDGFRα as proneural marker, transforming growth factor-beta (TGF-β) as the epithelial mesenchymal transformation's marker and HIF1α as the hypoxic marker (24).

TABLE 2. Patients Characteristics

Characteristics	$n = 52$
Median age, years (range)	65.9 (33–86)
Sex, n (%)	
Male	34 (65.4%)
Female	18 (34.6%)
Localization, n (%)	
Frontal	21 (40.4%)
Temporal	18 (34.6%)
Parietal	9 (17.3%)
Others	4 (7.7%)
Median KPS at preoperation (range)	74.0 (30–90)
Surgical procedure, n (%)	
Gross total resection	33 (63.4%)
Partial resection	19 (36.6%)

Abbreviations: KPS, Karnofsky Performance Status.

RESULTS

Clinical Data

A summary of the clinical information for the 52 patients with glioblastomas is shown in Table 2. The median age at diagnosis was 65.9 (33–86) years and 18 cases (34.6%) were female, 34 cases (65.4%) male. The median KPS at diagnosis was 74.0 (30–90) years. Tumors were localized to the frontal lobe in 21 cases, the temporal lobe in 18 cases, the parietal lobe in 9 cases, and in other regions for the remaining 4 cases. All patients received surgical treatment, followed by chemoradiotherapy with temozolomide.

Expression of GLUT1

Our study showed that GLUT1 was expressed on tumor cell membranes in all 52 cases, supporting previous reports (13, 19). The intensity of staining could be divided into 3 categories, mild (grade 1; Fig. 1B), moderate (grade 2; Fig. 1C), or strong (grade 3; Fig. 1D). Six high-power fields in each tissue samples were randomly selected and used to calculate the ratio of grades 2–3 assessments across the tumor sample. We defined a ratio of >20% between grades 2 and 3 as the high GLUT1 expression group, whereas ratios <19% were defined as a low expression group. Using these criteria, high expression of GLUT1 was detected in 16 cases and low expression was detected in 36 cases. Using an RNAscope system, *SLC2A1* mRNA was detected in glioblastoma tumor cells as either brown distinct points or clustered patterns (Fig. 2). A semiquantitative 4-level staining score was established for the RNAscope data. Samples defined as grades 3 or 4 (high expression) in the RNAscope study were the same as the GLUT1 high expression samples. In contrast, RNAscope staining

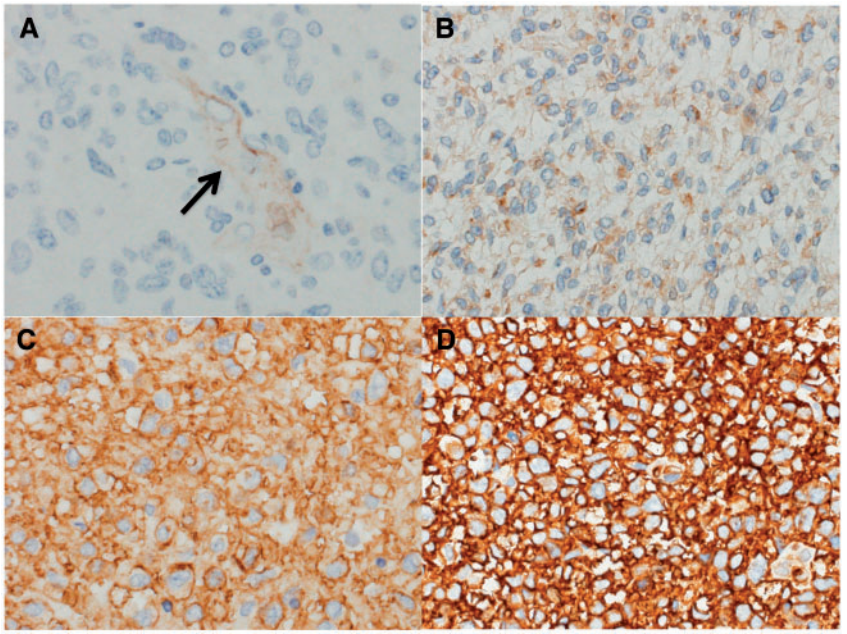

FIGURE 1. Immunohistochemical intensity scores of GLUT1 staining in glioblastoma tumor cells. GLUT1 was found to be expressed at the tumor cell membranes in glioblastomas. The staining intensity scores were evaluated according to a 4-grade system. **(A)** Negative cases showed no staining in tumor cells but were positive in endothelium for GLUT1 (arrow), whereas tumor cell membranes were stained to varying degrees in positive cases and were divided into grade 1 (**B,** mild), grade 2 (**C,** moderate), and grade 3 (**D,** strong) staining.

scores of grades 1 or 2 (low expression) were found in the GLUT1 low expression group. These data confirm that both GLUT1 and *SLC2A1* mRNA expression differ in glioblastomas and that there is an association between protein and transcript.

Localization of GLUT1

We next assessed the localization of GLUT1-positive cells in tissues, revealing that GLUT1 cells were located among perivascular and pseudopalisading cells and in tumor cells at the boundary between tumors and normal brain tissue (Fig. 3). Of note, GLUT1-positive cells were more commonly found at the perivascular region, in addition to pseudopalisades and tumor boundaries (Fig. 3D). This suggests that GLUT1 expression is associated with these migratory and hypoxic areas, indicating a link with glycometabolism. To show localized GLUT1 expression, double immunofluorescence was performed. Glioblastoma cells expressing GLUT1 were observed around CD34-positive blood vessels (Fig. 4A). Furthermore, GLUT1 and HIF1α were co-expressed in pseudopalisading necrosis (Fig. 4B). These findings supported the specific localization of GLUT1 expression in hypoxic areas of glioblastomas.

Association Between GLUT1 Expression, Angiogenesis, and Proliferation

Next, CD105 staining was used as a marker to distinguish between normal vessels and malignant intratumoral neovascularization to assess any correlation between high GLUT1 expression and angiogenesis. Averages of CD105-stained cell counts from 3 areas were recorded as CD105 intratumoral vessel density to compare the degree of angiogenesis. This showed that GLUT1 in the high expression group more frequently associated with CD105-positive vessels relative to the low GLUT1 expression group (Fig. 5A). The number of CD105-positive vessels positively correlated with the number of GLUT1-positive cells in the high expression tumors (correlation coefficient: 0.61). We also measured if there was any correlation between the expression of GLUT1 and tumor cell proliferation in glioblastomas using MIB-1 labeling indices. MIB-1 staining was immunohistochemically evaluated across continuous sections, revealing that the MIB-1 labeling indices in the high GLUT1 expression group were higher than that in the low expression group (Wilcoxon test: $p < 0.001$; Fig. 5B). Furthermore, double fluorescent immunostainings for GLUT1 and MIB-1 suggested that tumor cells with high proliferative potency expressed GLUT1 (Fig. 4C). Together, these data indicate a link between GLUT1 angiogenesis and glioblastoma cell proliferation.

Cell Proliferation and Viability

GLUT1 expression of U87, U251, and T98 cells was confirmed by Western blot analysis (data not shown). The viability of T98 and U87 with WZB-117 decreased in a concentration-dependent manner (Fig. 6A, B), whereas that of U251 decreased at 5 μM of WZB-117 (Fig. 6C).

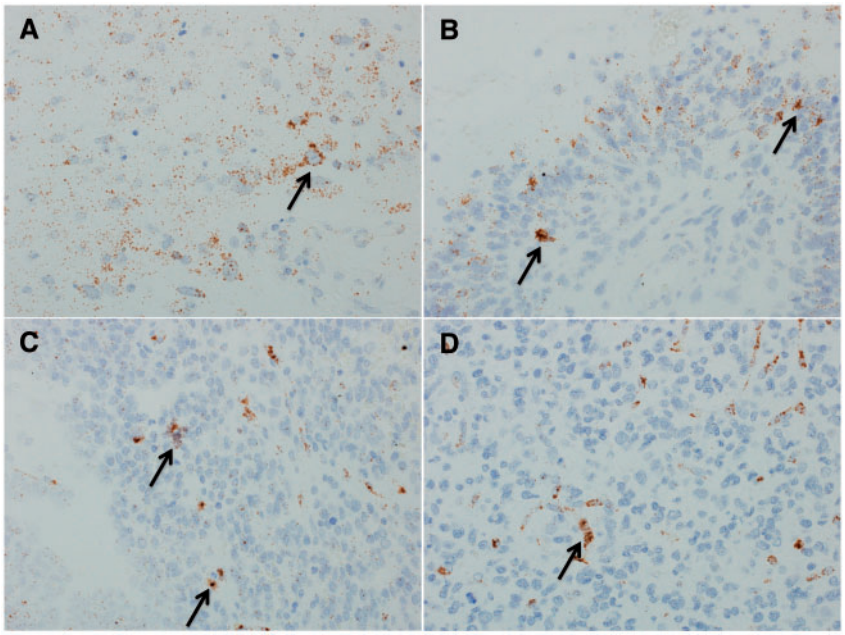

FIGURE 2. RNAscope in situ hybridization showing *SLC2A1* (*GLUT1*) mRNA expression in high GLUT1 expression samples. Tumor cells surrounding areas of necrosis or vessels that had >10 dots/cell **(A)** or 10% positive cells **(B)** with staining clusters (arrows) were assigned a score of 4. Tumor cells with >10 dots/cell **(C)** or <10% positive cells **(D)** with clusters (arrows) were given a score of 3.

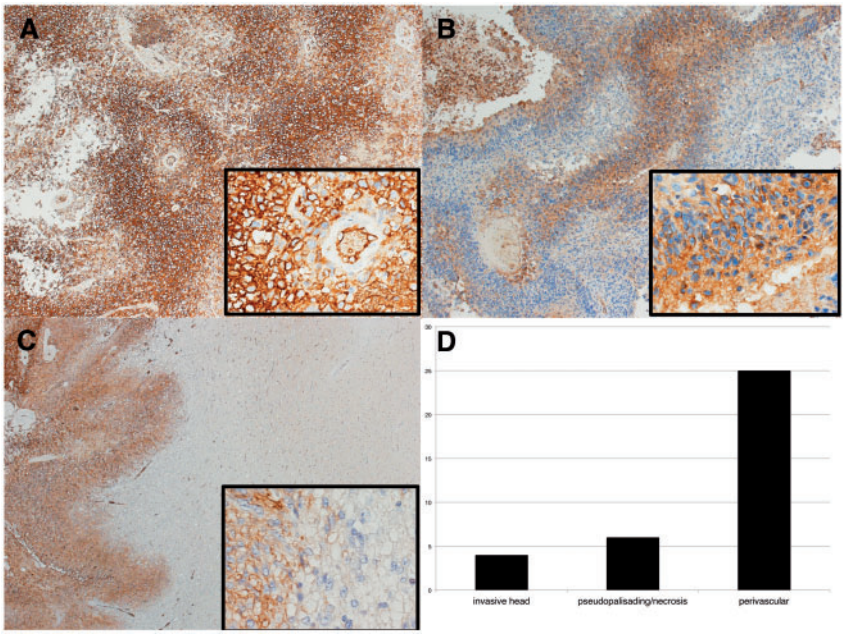

FIGURE 3. Localization of GLUT1 expression in glioblastoma tumor cells. (**A**) Immunohistochemical staining showed that GLUT1 was expressed predominantly perivascular region. GLUT1 staining was found around vessels (arrow) and formed a mottled pattern. (**B**) GLUT1 was also expressed in pseudopalisades of the tumor cell and (**C**) boundary area. (**D**) Number of cases in each localized expression of GLUT1. GLUT1-positive cells were most often observed at the perivascular regions. GLUT1 positive cells were also seen in pseudopalisades and at the boundaries between tumor and normal brain tissue. Cases are overlapping.

Association Between GLUT1 Expression and Patient Survival

Finally, Kaplan-Meier survival curve analysis indicated that the high GLUT1 expression group had lower overall survival rates than the low expression group (log-rank test: $p = 0.001$; Fig. 6D). There were no differences between progression-free survival rates in the high and low expression groups (data not shown). A further multivariate analysis

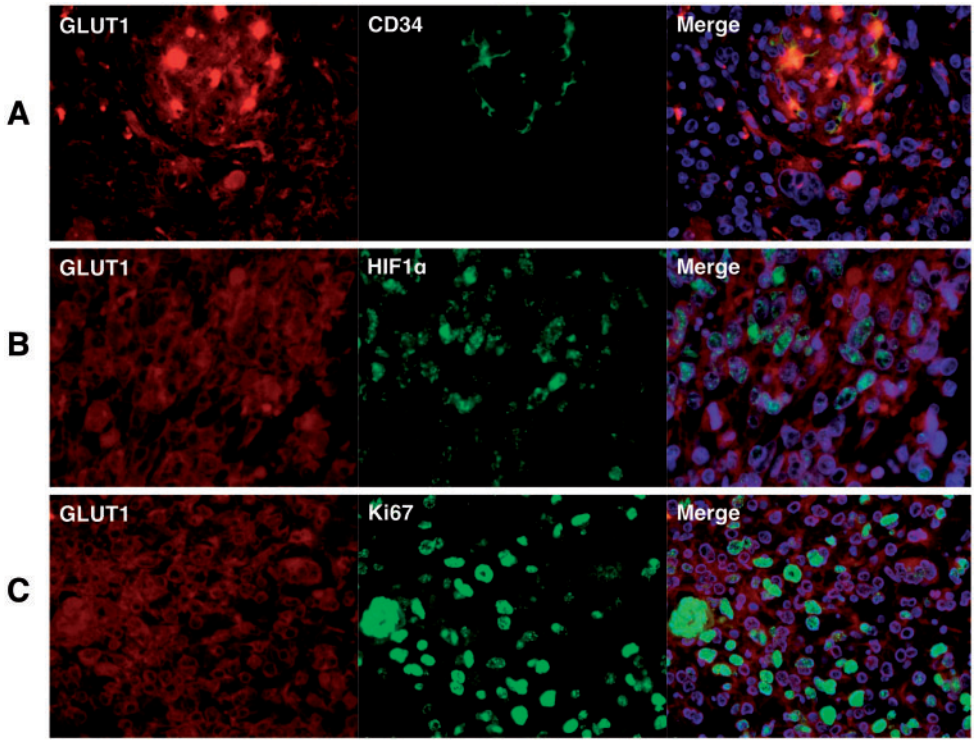

FIGURE 4. Double immunofluorescent staining of GLUT1 and other markers. **(A)** GLUT1 staining (left) and CD34 staining (center). Merged image (right) showed GLUT1 expression (red) around CD34 (green)-positive vessels. **(B)** GLUT1 staining (left) and HIF1α staining (center). Merged image (right) showed GLUT1 expression (red) around HIF1α (green) positive cells. **(C)** GLUT1 staining (left) and Ki67 staining (center). Merged image (right) showed co-expression of GLUT1 and Ki67 (green) in tumor cells.

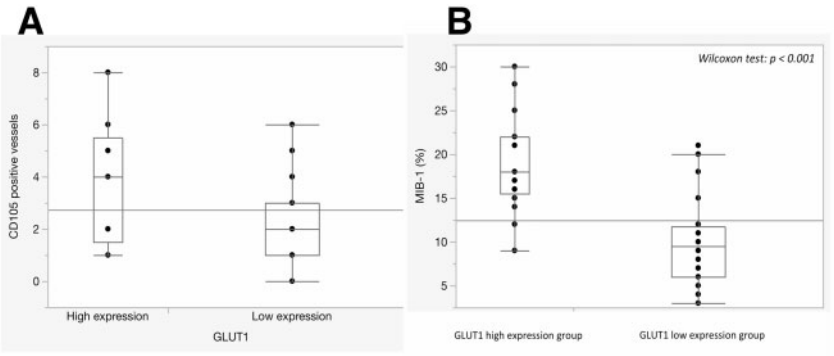

FIGURE 5. (A) Correlation between GLUT1 expression and angiogenesis. Cases with high GLUT1 expression possessed more CD105-positive vessels (Wilcoxon test $p < 0.001$). In addition, high GLUT1 expression positively correlated with the number of CD105-positive vessels (correlation coefficient: 0.61). **(B)** Correlation between GLUT1 expression and proliferative capacity. The MIB-1 labeling indices of the high GLUT1 expression group were higher than the low expression group (Wilcoxon test $p < 0.001$). In addition, high GLUT1 expression positively correlated with MIB-1 labeling indices (correlation coefficient: 0.51).

showed that GLUT1 was an independent predictor for poor prognosis when compared with already known prognostic factors, such as age or KPS (Table 3; hazard ratio 5.59, 95% confident interval 2.22–14.4, $p = 0.0003$). This suggests that GLUT1 is a novel independent predictor for glioblastoma outcome.

Gene Expression Database

To validate the result of the present study, data from TCGA database regarding GLUT1 in glioblastomas were analyzed (Supplementary Data). Two hundred and forty-nine cases (42%) showed upregulated SLC2A1 in 591 glioblastomas from TCGA database. The overall survival of upregulated

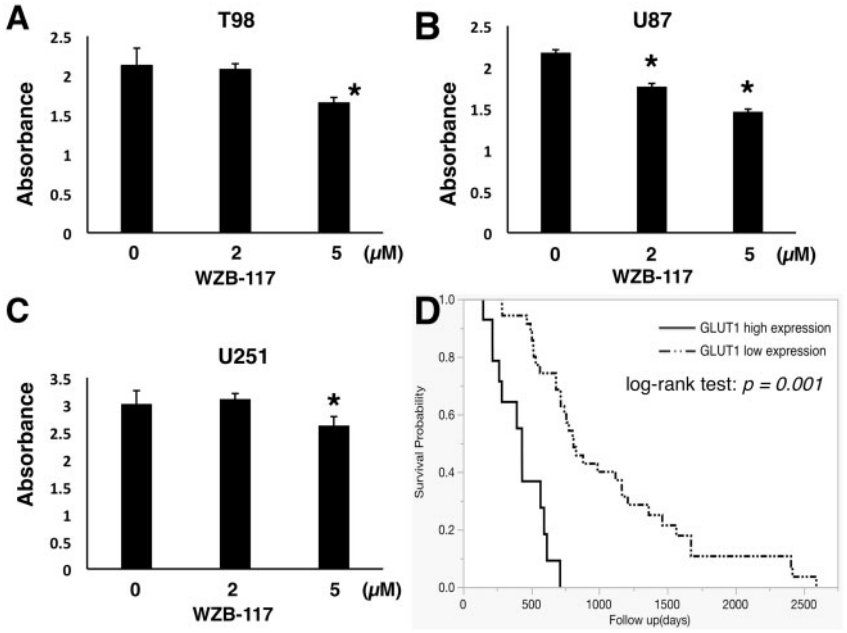

FIGURE 6. WST-1 cell proliferation assay and comparison of the Kaplan-Meier survival curves by GLUT1 expression. **(A–C)** U87, U251, and T98 cells were incubated in WZB-117 of indicated concentrations for 24 hours. Cell viability decreased in all tested cell lines in various manners. **(D)** Comparison of the Kaplan-Meier survival curves between the high and low GLUT1 expression groups showed that the high GLUT1 expression patient group had lower overall survival rates than the low expression group (log-rank test, p = 0.001).

TABLE 3. Univariate and Multivariate Predictors of Overall Survival

	Univariate			Multivariate		
Variables	**HR**	**95% CI**	**p Value**	**HR**	**95% CI**	**p Value**
High expression of GLUT1	7.22	3.05–17.3	<0.0001	5.59	2.22–14.4	0.0003
KPS <90	1.93	1.01–3.93	0.04	1.54	0.75–3.32	0.23
Age >50	2.05	0.91–5.53	0.09	1.86	0.75–5.44	0.18
Except gross total resection	1.13	0.58–2.12	0.69	1.04	0.50–2.06	0.89

Abbreviations: CI, confidence interval; KPS, Karnofsky Performance Status; HR, hazard ratio.

cases tended to be shorter than the not altered cases (Log-rank test; p = 0.375, Supplementary Data Fig. S1A), and the progression-free survival of upregulated cases was significantly shorter than the not altered cases (Log-rank test; p = 0.01, Supplementary Data Fig. S1B). SLC2A1 correlated with VEGF (Spearman's correlation coefficient 0.63, Supplementary Data Fig. S2A), TGF-β (Spearman's correlation coefficient 0.35, Supplementary Data Fig. S2B), and HIF1α (Spearman's correlation coefficient 0.33, Supplementary Data Fig. S2C). CD44 and PDGFRα did not show significant correlation with SLC2A1. These data from genome-wide analyses implied that GLUT1 was related with angiogenesis and hypoxia in glioblastomas overall.

DISCUSSION

It has previously been shown that glioblastomas are in a relatively hypoxic state with a degree of undernutrition due to their high proliferative potency and invasive capacity (25, 26). This assessment has been supported by several studies that have reported hypoxic environments in glioblastomas (16–20, 27). Using these data and a reverse interpretation of the Pasteur effect, it can be inferred that the energy metabolism of glioblastomas under hypoxia would depend on the glycolytic system (28). Angiogenesis elicited by such hypoxia would result in an aerobic environment and the glycolytic system of these tumor cells would be enhanced by the Warburg effect (28). However, irrespective of whether tumor cells are under an aerobic or anaerobic condition, tumor cells require an enormous amount of glucose to meet their energy requirements. Our study indicates that glioblastoma cells upregulate the GLUT1 transporter to promote glucose uptake in order to meet these high requirements. The present study also suggests a correlation between GLUT1 expression and MIB-1 labeling indices, suggesting a link between cell proliferation and the transporter. GLUT1 expression was observed in high proliferative glioblastoma cells positive for MIB-1 (Fig. 4C).

In our study, GLUT1 expression was evaluated in IDH wild-type glioblastomas using immunohistochemistry (to evaluate protein expression) and RNAscope in situ hybridization (to evaluate transcript expression). RNAscope allows single molecule visualization in individual cells to be achieved through the use of a novel probe design strategy and a hybridization-based signal amplification system that sup-

presses background noise (29). Previously, a number of studies have reported a link between certain mRNAs and cancer. Among them, Wang et al reported the efficacy of the RNAscope technique for examining invasive breast carcinomas that compared it to real-time quantitative PCR (qPCR) and other US Food and Drug Administration-approved methods, including fluorescence in situ hybridization (FISH) (30). Both RNAscope and qPCR data matched the FISH analysis in 97.3% of cases, showing that RNAscope is as accurate as qPCR and FISH (30). Importantly, the RNAscope approach can be used with archived FFPE tissues on glass slides and can be visualized either under a standard bright-field microscope (with chromogenic labels) or an epifluorescent microscope. A clear advantage of RNAscope is therefore its ability to visualize localized mRNA expression in samples. In the current study, GLUT1 protein expression was found to localize to glioblastoma cells and this was supported by our RNAscope analysis of *SLC2A1* expression (Fig. 5). Highly stained samples in the GLUT1 high expression group had similarly high *SLC2A1* scores. Conversely, the GLUT1 low expression group had lower *SLC2A1* scores.

Our study also revealed that GLUT1 expression was mainly localized to perivascular tumor cells. There was also a positive correlation between GLUT1 expression and neoangiogenesis highlighted by CD105 (endoglin) staining. CD105 is a 180 kDa integral membrane glycoprotein that is an accessory component of the TGF-β receptor complex. Applying analysis of CD105 expression to distinguish between normal vessels and malignant neovascularization has previously been reported, supporting our interpretation (31–33). The protein is predominantly expressed on cellular lineages within the vascular system, although it is more highly expressed by proliferating endothelial cells that participate in tumor angiogenesis. This pattern may emerge due to relatively lower expression in the vascular endothelium of normal tissues (34, 35). Markowski et al also reported that the expression levels of *HIF-1α*, *SLC2A1* (*GLUT1*), and *CD105* were higher in a group of patients with bladder cancer when compared with healthy subjects (33). The validation of the positive correlation of SLC2A1 and VEGF from TCGA database and GLUT1 expression around CD34-positive vessels suggested GLUT1 was related to tumor neoangiogenesis. Combined, these data indicate that there is a link between GLUT1 and endoglin expression, suggesting that the glycolytic system that emerges during glioblastoma development is accelerated by neoangiogenesis.

In addition, our examination of the localization of GLUT1 within tumor tissues revealed an association with pseudopalisade formation and microvascular proliferation, both pathological features of glioblastomas. The generation of pseudopalisades (hypercellular zones surrounding necrotic tissue) often results from the migration of glioma cells outwards from hypoxic areas due to vascular occlusion (36). Epithelial-mesenchymal transition (EMT) is the process by which epithelial cells lose cell polarity and adhesiveness and is one of the main mechanisms that exacerbates tumor migration in glioblastomas (37). The zinc finger E-box-binding homeobox (ZEB) proteins, ZEB1, and smad1-interacting protein-1 (also known as ZEB2), are members of a family of noteworthy transcription factors that are responsible for the mediation of EMT in numerous types of cancer including glioma (38). Chem et al detected the expression of ZEB1 and ZEB2 in 91 cases of GBM with immunohistochemistry (39). The percentages of ZEB1 high expression and ZEB2 high expression were 31.9% (29/91) and 41.9% (36/91), respectively. They revealed that high expression of ZEB2 was significantly associated with lower survival rate of GBM patients ($p = 0.001$). Justin et al revealed hypoxia-induced mesenchymal shift in GBM primary material by showing colocalization of GLUT1, ZEB1 and the mesenchymal marker YKL40 in hypoxic regions of the tumor (40). These results suggested that GLUT1 may exist downstream of the ZEB1 pathway; further studies are needed to clarify the relationship GLUT1 and ZEB1. In previous reports, GLUT1 has been found to associate with lymph node metastasis and is also highly expressed by breast cancer cells (10, 41). These studies also reported that GLUT1 expression contributed to increased tumor viability by promoting glycolysis. The results showing that GLUT1 is expressed in both hypoxic and proliferative area suggested that glioblastoma cells increased their proliferative potency via hypoxic stress.

These studies, in combination with our own analysis showing GLUT1 localization at tumor pseudopalisades, indicate a possible link to EMT. We therefore hypothesize that tumor malignancy in glioblastomas may be increased by GLUT1 through higher migration and invasiveness.

Finally, Kaplan-Meier survival curve analysis revealed that survival in the high GLUT1 expression group was lower than the low expression group. Our multivariate analysis also showed that GLUT1 was an independent predictor for worse prognoses compared with already known prognostic factors, including age and KPS. These data suggest that GLUT1 may act as an independent prognostic factor for glioblastoma due to an accelerated glycolytic system, likely through increased neoangiogenesis and the Warburg effect. This would subsequently increase migration and invasiveness by promoting EMT. Previously, Phadngam et al reported that GLUT1 acts downstream of the PI3K-Akt pathway (28) and several studies have suggested a link between GLUT1, HIF1α, and GSK3β, although the exact details remain unclear. For example, Azzalin et al reported that various inhibitors of GLUT/SLC2A enhance the activity of the chemotherapeutic agents bis-chloroethylnitrosourea (BCNU) and temozolomide against high-grade gliomas (42). Chen et al also reported that specific blockade of GLUT1 using WZB117 resensitizes breast cancer cells to adriamycin (43). In the present study, GLUT1 inhibition by WZB-117 decreased cell viability in cell lines. There is a considerable potential for the therapeutic application of GLUT1 inhibitors against glioblastoma, but further experiments, for example, whether WZB-117 potentiate temozolomide and/or irradiation, are required.

In conclusion, our study has revealed that GLUT1 is a biomarker and predictor for a worse prognostic outcome in patients with glioblastomas. This will assist the development and application of tools and treatment to better target vulnerable patients. However, recent advancements suggest that

GLUT1 also has the potential to increase the efficacy of various anticancer agents. Therefore, our study reveals several important characteristics of GLUT1 expression in glioblastomas.

ACKNOWLEDGMENT

We would like to thank Editage (www.editage.jp) for English language editing.

REFERENCES

1. Wood IS, Trayhurn P. Glucose transporters (GLUT and SGLT): Expanded families of sugar transport proteins. BJN 2003;89:3–9
2. Uldry M, Thorens B. The SLC2 family of facilitated hexose and polyol transporters. Pflugers Arch 2004;447:480–9
3. Pao SS, Paulsen IT, Saier MH Jr. Major facilitator superfamily. Microbiol Mol Biol Rev 1998;62:1–34
4. Simpson IA, Vannucci SJ, DeJoseph MR, et al. Glucose transporter asymmetries in the bovine blood-brain barrier. J Biol Chem 2001;276:12725–9
5. Bannasch D, Safra N, Young A, et al. Mutations in the *SLC2A9* gene cause hyperuricosuria and hyperuricemia in the dog. PLoS Genet 2008;4: e1000246
6. Mueckler M, Caruso C, Baldwin SA, et al. Sequence and structure of a human glucose transporter. Science 1985;29:941–5
7. Younes M, Lechago LV, Lechago J. Overexpression of the human erythrocyte glucose transporter occurs as a late event in human colorectal carcinogenesis and is associated with an increased incidence of lymph node metastases. Clin Cancer Res 1996;2:1151–4
8. Cooper R, Sarioğlu S, Sökmen S, et al. Glucose transporter-1 (GLUT-1): A potential marker of prognosis in rectal carcinoma? Br J Cancer 2003; 89:870–6
9. Haber RS, Rathan A, Weiser KR, et al. GLUT1 glucose transporter expression in colorectal carcinoma: A marker for poor prognosis. Cancer 1998;83:34–40
10. Mayer A, Hockel M, Wree A, et al. Microregional expression of glucose transporter-1 and oxygenation status: Lack of correlation in locally advanced cervical cancers. Clin Cancer Res 2005;11:2768–73
11. de Wit M, Jimenez CR, Carvalho B, et al. Cell surface proteomics identifies glucose transporter type 1 and prion protein as candidate biomarkers for colorectal adenoma-to-carcinoma progression. Gut 2012;61:855–64
12. McKinnon B, Bertschi D, Wotzkow C, et al. Glucose transporter expression in eutopic endometrial tissue and ectopic endometriotic lesions. J Mol Endocrinol 2014;52:169–79
13. Osugi J, Yamaura T, Muto S, et al. Prognostic impact of the combination of glucose transporter 1 and ATP citrate lyase in node-negative patients with non-small lung cancer. Lung Cancer 2015;88:310–8
14. Sun XF, Shao YB, Liu MG, et al. High-concentration glucose enhances invasion in invasive ductal breast carcinoma by promoting Glut1/MMP2/MMP9 axis expression. Oncol Lett 2017;13:2989–95
15. Wang J, Ye C, Chen C, et al. Glucose transporter GLUT1 expression and clinical outcome in solid tumors: A systematic review and meta-analysis. Oncotarget 2017;8:16875–86
16. Mayer A, Schneider F, Vaupel P, et al. Differential expression of HIF-1 in glioblastoma multiform and anaplastic astrocytoma. Int J Oncol 2012; 41:1260–70
17. Inukai M, Hara A, Yasui Y, et al. Hypoxia-mediated cancer stem cells in pseudopalisades with activation of hypoxia-inducible factor-1α/Akt axis in glioblastoma. Hum Pathol 2015;46:1496–505
18. Evans SM, Judy KD, Dunphy I, et al. Hypoxia is important in the biology and aggression of human glial brain tumors. Clin Cancer Res 2004;10:8177–84
19. Kaur B, Khwaja FW, Severson EA, et al. Hypoxia and the hypoxia-inducible-factor pathway in glioma growth and angiogenesis. Neuro-Oncol 2005;7:134–53
20. Kessler J, Hahnel A, Wichmann H, et al. HIF-1alpha inhibition by siRNA or chetomin in human malignant glioma cells: Effects on hypoxic radioresistance and monitoring via CA9 expression. BMC Cancer 2010;10:605
21. Louis DN, Ohgaki H, Wiestler OD, et al. WHO Classification of Tumours of the Central Nervous System. Lyon: International Agency Research on Cancer 2016
22. Cerami E, Gao J, Dogrusoz U, et al. The cBio Cancer Genomics Portal: An open platform for exploring multidimensional cancer genomics data. Cancer Discov 2012;401–4
23. Gao J, Aksoy BA, Dogrusoz U, et al. Integrative analysis of complex cancer genomics and clinical profiles using the cBioPortal. Sci Signal 2013;6:269
24. Ozawa T, Riester M, Cheng YK, et al. Most human non-GCIMP glioblastoma subtypes evolve from a common proneural-like precursor glioma. Cancer Cell 2014;26:288–300
25. Oudard S, Arvelo F, Miccoli L, et al. High glycolysis in gliomas despite low hexokinase transcription and activity correlated to chromosome 10 loss. Br J Cancer 1996;74:839–45
26. Tabatabaei P, Bergström P, Henriksson R, et al. Glucose metabolites, glutamate and glycerol in malignant glioma tumours during radiotherapy. J Neurooncol 2008;90:35–9
27. Joseph JV, Conroy S, Pavlov K, et al. Hypoxia enhances migration and invasion in glioblastoma by promoting a mesenchymal shift mediated by the HIF1α-ZEB1 axis. Cancer Lett 2015;359:107–16
28. Phadngam S, Castiglioni A, Ferraresi A, et al. PTEN dephosphorylates AKT to prevent the expression of GLUT1 on plasmamembrane and to limit glucose consumption in cancer cells. Oncotarget 2016;7: 84999–5020
29. Wang F, Flanagan J, Su N, et al. RNAscope: A novel in situ RNA analysis platform for formalin-fixed, paraffin-embedded tissues. J Mol Diagn 2012;14:22–9
30. Wang Z, Portier BP, Gruver AM, et al. Automated quantitative RNA in situ hybridization for resolution of equivocal and heterogeneous ERBB2 (HER2) status in invasive breast carcinoma. J Mol Diagn 2013;15:210–9
31. Dallas NA, Samuel S, Xia L, et al. Endoglin (CD105): A marker of tumor vasculature and potential target for therapy. Clin Cancer Res 2008;14: 1931–7
32. Sica G, Lama G, Anile C. Assessment of angiogenesis by CD105 and nestin expression in peritumor tissue of glioblastoma. Int J Oncol 2011; 38:41–9
33. Markowski M, Lipiński M, Krzeslak A, et al. HIF-1, GLUT1, endoglin, and BIRC5 expression in urine samples obtained from patients with bladder malignancies – after photodynamic diagnosis (PDD). Cent Eur J Urol 2012;65:146–50
34. Duff SE, Li C, Garland JM, et al. CD105 is important for angiogenesis: Evidence and potential applications. FASEB J 2003;17:984–92
35. Yao Y, Kubota T, Takeuchi H, et al. Prognostic significance of microvessel density determined by an anti-CD105/endoglin monoclonal antibody in astrocytic tumors: Comparison with an anti-CD31 monoclonal antibody. Neuropathology 2005;25:201–6
36. Brat DJ, Van Meir EG. Vaso-occlusive and prothrombotic mechanisms associated with tumor hypoxia, necrosis, and accelerated growth in glioblastoma. Lab Invest 2004;84:397–405
37. Iwatabe Y. Epithelial-mesenchymal transition in glioblastoma progression (Review). Oncol Lett 2016;11:1615–20
38. Wang Q, Li X, Zhu Y, et al. MicroRNA-16 suppresses epithelial-mesenchymal transition-related gene expression in human glioma. Mol Med Rep 2014;10:3310–4
39. Chen P, Liu H, Hou K, et al. Prognostic significance of zinc finger E-box-binding homeobox family in glioblastoma. Med Sci Monit 2018;24: 1145–51
40. Justin V, Siobhan Conroy, Kirill Pavlov, et al. Hypoxia enhances migration and invasion in glioblastoma by promoting a mesenchymal shift mediated by the HIF1α-ZEB1 axis. Cancer Lett 2015:359:107–16
41. Li W, Wei Z, Liu Y, et al. Increased 18F-FDG uptake and expression of Glut1 in the EMT transformed breast cancer cells induced by TGF-β. Neoplasma 2010;57:234–40
42. Azzalin A, Nato G, Parmigiani E, et al. Inhibitors of GLUT/SLC2A Enhance the Action of BCNU and Temozolomide against High-Grade Gliomas. Neoplasia 2017;19:364–73
43. Chen Q, Meng YQ, Xu XF, et al. Blockade of GLUT1 by WZB117 resensitizes breast cancer cells to Adriamycin. Anticancer Drugs 2017;28:880–7